Impurity-bound small polarons in ZnO: Hybrid density functional calculations

Mao-Hua Du[1] and S. B. Zhang[2]
[1]*Materials Science & Technology Division, Oak Ridge National Laboratory, Oak Ridge, Tennessee 37831, USA*
[2]*Department of Physics, Applied Physics, and Astronomy, Rensselaer Polytechnic Institute, Troy, New York 12180, USA*
(Received 24 July 2009; revised manuscript received 4 September 2009; published 30 September 2009)

Hybrid density functional calculations are performed to study the electronic and optical properties of substitutional Li and Na in ZnO. Our calculations correctly show hole localizations at neutral Li^0_{Zn} and Na^0_{Zn}, which lead to the formation of small polarons as observed experimentally. This is in contrast to previous local-density and generalized gradient calculations that showed delocalized holes. The calculated localization energies are, however, still noticeably smaller than the available experimental values. Our analysis of the discrepancies suggests that further improvement of the theory and a refinement of the experimental values are both required.

DOI: 10.1103/PhysRevB.80.115217 PACS number(s): 61.72.S−, 71.38.Ht, 71.55.Gs

I. INTRODUCTION

ZnO is a promising wide-gap semiconductor for blue/UV optoelectronics[1] and is also a fast scintillator that may be used for radiation detection.[2] Li is commonly found in ZnO single crystals grown by hydrothermal technique. Extensive research has been devoted to the studies of Li- and Na-induced defect states and possible *p*-type doping of ZnO using alkali-metal elements.[3–11]

ZnO is typically *n* type. Thus, Li_{Zn} and Na_{Zn} are negatively charged as Li^-_{Zn} and Na^-_{Zn}. Neutral Li^0_{Zn} and Na^0_{Zn} can be generated in ZnO under illumination. Electron paramagnetic resonance results show that the hole at Li^0_{Zn} or Na^0_{Zn} is localized at one of the four neighboring O atoms rather than delocalized around all the O neighbors.[4–6]

A delocalized carrier can self-trap by distorting lattice structure, forming a small polaron.[12,13] For instance, in alkali and alkaline-earth halides, holes self-trap to form V_k centers. In oxides, holes are often bound to the acceptor defects, e.g., cation vacancies and alkali impurities, and distort the local symmetry.[14] At Li^0_{Zn} in ZnO, the localization of the hole at the axial O ion along the *c* axis is energetically more stable by ~15 meV than at one of the three nonaxial O ions.[4] The hole localization reduces Coulomb attraction between the axial O ion and the Li ion, leading to an increase in their distance. For Na^0_{Zn}, however, the nonaxial center is found to be more stable than the axial center by $\Delta E \geq 25$ meV.[6]

The hole localization results in structural distortion and appearance of a deep level in the band gap. Luminescence data show emission peaks of 2.2 eV (Ref. 5) for Li_{Zn} and 2.18 eV (Ref. 6) for Na_{Zn}. Both Li_{Zn} and Na_{Zn} peaks are broad and strongly phonon coupled with half widths of 0.5 eV (Ref. 5) and 0.4 eV,[6] respectively. These results suggest that large phonon relaxation occurs upon change in charge state for Li_{Zn} and Na_{Zn}. No zero-phonon lines (ZPLs) were observed. By extrapolating the luminescence curves to high-energy limits, the ZPLs were estimated to be 2.6 eV for Li_{Zn} and 2.8 eV for Na_{Zn}, leading to their respective hole binding energy of 0.8 and 0.6 eV.[5,6]

In contrast to experimental results, calculations based on density functional theory (DFT) within local-density approximation (LDA) predict delocalized shallow hole state associated with Li^0_{Zn} and Na^0_{Zn} in ZnO.[9–11] The failure of DFT calculations with LDA or generalized gradient approximation (GGA) to predict small polaron formation had been observed before in several systems.[15–17] The LDA and GGA suffer from the well-known electron self-interaction due to its local exchange-energy approximation. The minimization of the artificial self-interaction often leads to artificial over-delocalization of orbitals. On the other hand, the Hartree-Fock (HF) calculations with exact exchange but no correlation usually overestimate the localization. Typically, the HF calculations give too large band gap and charge localization energy while LDA calculations give too small band gap and too small or no charge localization.

Recently, there has been increasing number of DFT calculations of defect properties in semiconductors using hybrid functionals,[18–26] such as B3LYP,[27] PBE0,[28] and HSE (Ref. 29) functionals, which include a fraction of HF exact exchange energy. These hybrid functionals improve the band-gap energy,[30,31] which is crucial to the prediction of the gap-state position. The B3LYP functional has also been used to predict carrier self-trapping in HfO_2.[18] In this paper, we report results of electronic and optical properties of Li_{Zn} and Na_{Zn} in ZnO based on all-electron hybrid density functional calculations. We show that Li^0_{Zn} and Na^0_{Zn} indeed induce deep hole states in the band gap.

II. COMPUTATIONAL METHODS

We performed hybrid DFT calculations using Crystal codes.[32] All-electron Gaussian basis sets were used for Zn,[33] O,[34] Li,[35] and Na.[36] The calculated ZnO band gap based on B3LYP functional is 3.26 eV. We slightly increase the percentage of HF exchange energy from 20% to 21.5% in the exchange-energy functional to increase the ZnO band gap to 3.4 eV, matching the experimental value. All the defect calculations were preformed using 96-atom supercells. A $2\times2\times2$ grid centered at Γ point was used for the *k*-point sampling of Brillouin zone. The calculated ZnO lattice constants are $a=3.286$ Å and $c=5.253$ Å, about 1% larger than the experimental values of $a=3.250$ Å and $c=5.207$ Å.[37]

The $(0/-)$ thermal transition energy level for A (=Li, Na) is given by

$$\varepsilon(0/-) = E(A^-) - E(A^0) - \varepsilon_{\mathrm{VBM}}, \quad (1)$$

where $E(A^-)$ and $E(A^0)$ are total energies of supercells that contain relaxed structures of A^- and A^0, respectively. The

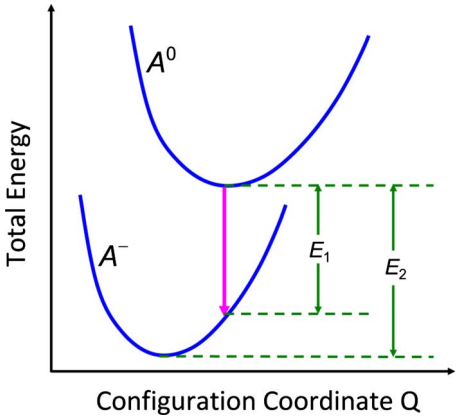

FIG. 1. (Color online) Configuration coordinate diagram for recombination between a shallow-donor electron and a hole trapped at a deep acceptor, A (=Li or Na). The electron vertical transition to the deep hole level that is induced by the relaxed structure of A^0 releases a photon of energy E_1, which is related to the calculated vertical transition level $E_g - E_1$ (E_g is the band-gap energy). The zero-phonon line corresponds to luminescence energy of E_2, which can be related to the calculated thermal transition level $E_g - E_2$.

valence-band maximum (VBM) energy, ε_{VBM}, is defined as $E(H^0) - E(H^+)$, where $E(H^0)$ and $E(H^+)$ are the total energies of host ZnO supercells at neutral and (+) charge states, respectively. For neutral Li^0_{Zn} and Na^0_{Zn}, spin-polarized hybrid DFT calculations were performed.

The (0/−) vertical transition levels for luminescence can also be calculated using Eq. (1) but with $E(A^-)$ calculated at the relaxed structure of A^0 rather than A^-. The thermal and vertical transition levels defined above correspond to $E_{gap} - E_2$ and $E_{gap} - E_1$, where E_2 and E_1 are shown in Fig. 1 and E_{gap} is the band-gap energy. E_1 can be compared with the experimentally observed luminescence peak and E_2 can be compared with ZPL. The ZPLs for Li_{Zn} and Na_{Zn} in ZnO have not been observed but have been estimated.

III. RESULTS

A. Li_{Zn}

In typical n-type ZnO, Li_{Zn} is negatively charged as Li^-_{Zn}. The calculated Li-O bond length is about 2.01 Å, nearly same as the calculated Zn-O bond length of 2.00 Å. This is expected due to the nearly same Shannon (ionic) radii of fourfold coordinated Zn^{2+} and Li^+, which are 0.74 and 0.73 Å, respectively.[38] For Li^0_{Zn}, structural optimization within the hybrid-functional formalism reveals that the hole can be localized at either the axial or nonaxial O ions next to the Li. This is distinctly different from the LDA and GGA calculations[9,11] which show delocalized holes at Li^0_{Zn}. Figure 2(a) shows the optimized structure of the axial center of Li^0_{Zn}. The hole localization increases the distance between the Li and axial O to 2.61 Å, a 31% increase compared to bulk Zn-O bond length. The Li and axial O ions relax away from each other. The bond lengths between the Li and nonaxial O ions decrease to 1.90 Å. The calculated densities of states (see Fig. 3) show the splitting of the spin-up and spin-down

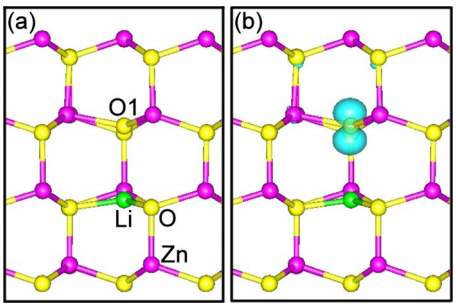

FIG. 2. (Color online) Structure of (a) axial Li^0_{Zn} and (b) partial charge-density contour (0.1 $e^-/Å^3$) of the hole state deep inside the ZnO band gap (see text).

states of the O orbitals. A deep hole level [mainly derived from the axial O ion next to the Li, i.e., O1 in Fig. 2(a)] appears inside the band gap. Figure 2(b) shows the partial charge-density contour for the hole gap state in Fig. 3. Clearly, this state is the O 2p orbital localized at the axial O atom.

The hole at Li^0_{Zn} can also be localized at the nonaxial O ion next to the Li, leading to an elongation of the Li-O distance to 2.60 Å, similar to the case of the axial center. Our calculations show that Li^0_{Zn} (axial) is less stable than Li^0_{Zn} (nonaxial) by 14 meV, which is opposite to the experimental finding that the former is more stable than the latter by 15 meV (Ref. 4). However, these are very small energy differences that cannot be resolved by typical DFT calculations with error bars up to 100 meV. The optical hole ionization energies for both the axial and nonaxial Li^0_{Zn} are at about $\varepsilon_{VBM}+1.0$ eV (with the calculated difference of only 7 meV). These energies correspond to the luminescence energy of 2.4 eV, which agrees with the measured luminescence peak position of 2.2 eV.[5]

We have also calculated the energy for Li^0_{Zn} without the structural distortion, corresponding to the delocalized hole. A comparison shows that the hole localization lowers the total energy by only about 0.2 eV, which suggests that the energy gain by the electron-lattice coupling is largely offset by the energy cost of kinetic energy and strain energy. The (0/−) thermal transition level is calculated to be $\varepsilon_{VBM}+1.2$ eV. We have also calculated the (0/−) thermal transition level for the undistorted Li_{Zn} with delocalized hole, which yields a value

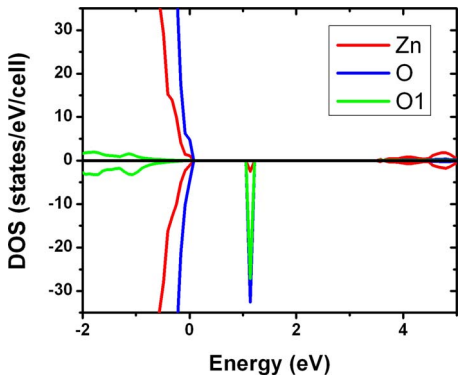

FIG. 3. (Color online) Density-of-states projected to all Zn atoms, all O atoms, and the axial O atom next to Li [O1 in Fig. 2(a)].

TABLE I. Calculated and measured $(0/-)$ transition levels for Li_{Zn} and Na_{Zn} in ZnO. The vertical and thermal $(0/-)$ levels are defined as E_g-E_1 and E_g-E_2, respectively, where E_g is the band-gap energy, E_1 and E_2 are schematically shown in Fig. 1. The relaxation energy is the difference between the vertical and thermal transition levels, i.e., E_2-E_1. Note that thermal transition levels have not been accurately measured. They are the hypothetical zero-phonon lines estimated by extrapolating the luminescence curves to the high-energy limits.

	Li_{Zn}			Na_{Zn}		
	Theory	Experiment (Ref. 5)	Difference	Theory	Experiment (Ref. 6)	Difference
Vertical transition level E_g-E_1	1.0	1.2	−0.2	0.7	1.2	−0.5
Thermal transition level E_g-E_2	0.3	0.8	−0.5	0.3	0.6	−0.3
Relaxation energy E_2-E_1	0.7	0.4	0.3	0.4	0.6	−0.2

of $\varepsilon_{VBM}-0.07$ eV. An acceptor level below the VBM is unphysical. However, these numbers should be revised to account for the small-supercell error. A small supercell corresponds to a high density of Li impurities that leads to a large dispersion of the impurity bands. The shallow Li_{Zn}^{-} band has relatively large dispersion and closely tracks the valence-band edge while the deep Li_{Zn}^{0} band has negligible dispersion in our calculations. The correction that accounts for the small-supercell errors is estimated to be 0.2 eV. This places the $(0/-)$ thermal transition level for the Li_{Zn} at about $\varepsilon_{VBM}+0.3$ eV.

For the $(0/-)$ vertical transition level, however, the small-supercell correction can be neglected because both Li_{Zn}^{0} and Li_{Zn}^{-} are fixed at relaxed Li_{Zn}^{0} structure and induce deep gap levels with negligible dispersions. The calculated $(0/-)$ vertical and thermal transition levels for Li_{Zn} are compared with the experimental values in Table I. The energy difference between the $(0/-)$ vertical and thermal transition levels is the structural relaxation energy after the recombination between a shallow-donor state and a deep acceptor state, which equals to E_2-E_1 in Fig. 1, and is about 0.7 eV for Li_{Zn}.

B. Na_{Zn}

The Shannon radius of Na^{+} (1.13 Å) is significantly larger than that of Zn^{2+} (0.74 Å). Thus, the Na-O bond at Na_{Zn}^{-} is calculated to be 2.20 Å, 10% longer than the Zn-O bond. The hole localization at Na_{Zn}^{0} can take place at either the axial or nonaxial O ion next to the Na. The nonaxial center is found to be more stable than the axial center by 0.11 eV, consistent with the experimental finding (Ref. 6). Figure 4(a) shows the structure of the nonaxial Na_{Zn}^{0}. The hole localization increases the Na-O1 bond length to 2.31 Å mainly due to the relaxation of the O1 atom while the other three Na-O bond lengths of about 2.18 Å are largely unchanged. The hole state of the Na_{Zn}^{0} also appears in the band gap similar to that of the Li_{Zn}^{0} in Fig. 3. The partial charge-density contour of this hole state [Fig. 4(b)] shows that it mainly consists of an O $2p$ orbital localized at the O1 atom [shown in Fig. 4(a)]. The calculated hole optical ionization energy is 0.7 eV, smaller than the experimental value of 1.2 eV (Ref. 6). The hole localization energy is calculated to be 0.1 eV. The $(0/-)$ thermal transition level is $\varepsilon_{VBM}+0.12$ eV, similar to Li_{Zn}. Following the discussion of small-supercell errors in Sec. III A, the $(0/-)$ thermal transition level is corrected to $\varepsilon_{VBM}+0.3$ eV. The calculated $(0/-)$ vertical and thermal transition levels for Na_{Zn} are compared with experimental values in Table I.

IV. DISCUSSION

The luminescence peaks for Li_{Zn} and Na_{Zn} in ZnO are close to each other as indicated in Table I. The calculated $(0/-)$ vertical transition levels are lower than the experimental values. The hole localization energies are calculated to be 0.2 eV for Li_{Zn} and 0.1 eV for Na_{Zn}. The formation of small polarons involves the interplay of several interactions. The electron-lattice coupling enhances the Coulomb attraction but the carrier localization increases kinetic and strain energies. The net energy lowering due to hole localization at Li_{Zn}^{0} or Na_{Zn}^{0} in ZnO appears to be still underestimated by our hybrid-functional DFT calculations. Increasing the percentage of the HF exchange energy will increase the hole localization and hence improve the agreement between theory and experiment. However, the properties of the ZnO host, such as lattice constant and band gap, will suffer. The optimal fractions of HF exchange energy may vary among different sys-

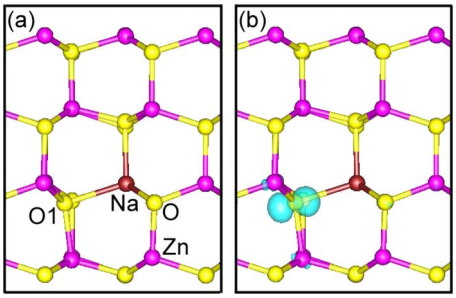

FIG. 4. (Color online) Structure of (a) nonaxial Na_{Zn}^{0} and (b) partial charge-density contour (0.1 $e^{-}/Å^{3}$) of the hole state deep inside the ZnO band gap (see text).

tems. The bulk materials and the point defects may also correspond to different optimal fractions of HF exchange energy. This intrinsic problem for calculating defect properties in solids using DFT is a general problem for approximated exchange and correlation energies (including LDA and GGA), which lead to different amount of errors for extended bulk states and localized defect states.

The calculated lattice distortion for Na_{Zn}^{0} is significantly smaller than that for Li_{Zn}^{0}, which is expected because Na is much larger than Li. The Na impurity applies a compressive strain on the ZnO lattice, which constrains the degree of structural relaxations upon bond breaking and hole localization. This fact is reflected in our calculations as a smaller hole vertical ionization energy and a smaller relaxation energy for Na_{Zn} than for Li_{Zn} (see Table I). In contrast, the experimentally estimated relaxation energy for Na_{Zn} is larger than that for Li_{Zn}. We note, however, that the estimated relaxation energy in Refs. 5 and 6 is simply the energy difference between the extrapolated high-energy limit and the peak of the luminescence curve, which may not be sufficiently accurate. A careful measurement on the Huang-Rhys factor by temperature-dependent luminescence experiments may give more reliable results on the relaxation energies.

In short, the current differences between the theoretical and experimental values of the $(0/-)$ transition levels for Li_{Zn} and Na_{Zn} in ZnO may be the results of two contributing factors: (1) the underestimated hole localization in the calculations and (2) the insufficient accuracy in the measurement of the relaxation energy.

V. CONCLUSION

We have performed the hybrid density functional calculations to study small polarons formed at neutral Li_{Zn}^{0} and Na_{Zn}^{0} in ZnO. In contrast to the delocalized hole states predicted by the LDA and GGA, our calculations show deep single-particle hole states for both the Li_{Zn}^{0} and Na_{Zn}^{0} inside the ZnO band gap. The calculated vertical transition levels for Li_{Zn} and Na_{Zn} are $\varepsilon_{VBM}+1.0$ eV and $\varepsilon_{VBM}+0.7$ eV, respectively, compared to the experimentally observed luminescence peaks at about $\varepsilon_{VBM}+1.2$ eV for both. The calculated localization energies appear to be smaller than the experimental values. The structural relaxation energies upon electron-hole recombination are 0.7 and 0.4 eV for Li_{Zn} and Na_{Zn}, respectively. These findings are consistent with the fact that the structural distortion at Li_{Zn} should be significantly larger than that at Na_{Zn}. Our results place the $(0/-)$ thermal transition levels for both Li_{Zn} and Na_{Zn} at about $\varepsilon_{VBM}+0.3$ eV. On the other hand, the experimentally estimated relaxation energies are 0.4 and 0.6 eV for Li_{Zn} and Na_{Zn}, respectively, which place the $(0/-)$ thermal transition levels at $\varepsilon_{VBM}+0.8$ eV and $\varepsilon_{VBM}+0.6$ eV, respectively.

ACKNOWLEDGMENTS

We thank B. K. Meyer for helpful discussions. This work was supported by U.S. DOE Office of Nonproliferation Research and Development NA22 and Oak Ridge National Laboratory LDRD program. Computations were performed at the DoD Major Shared Resource Center at ASC.

[1] K. Klingshirn, Phys. Status Solidi B **244**, 3027 (2007).
[2] W. W. Moses, Nucl. Instrum. Methods Phys. Res. A **487**, 123 (2002).
[3] J. J. Lander, J. Phys. Chem. Solids **15**, 324 (1960).
[4] O. F. Schirmer, J. Phys. Chem. Solids **29**, 1407 (1968).
[5] O. F. Schirmer and D. Zwingel, Solid State Commun. **8**, 1559 (1970).
[6] D. Zwingel and F. Gärtner, Solid State Commun. **14**, 45 (1974).
[7] E. Tomzig and R. Helbig, J. Lumin. **14**, 403 (1976).
[8] B. K. Meyer, H. Alves, D. M. Hofmann, W. Kriegseis, D. Forster, F. Bertram, J. Christen, A. Hoffmann, M. Straßburg, M. Dworzak, U. Haboeck, and A. V. Rodina, Phys. Status Solidi B **241**, 231 (2004).
[9] C. H. Park, S. B. Zhang, and S.-H. Wei, Phys. Rev. B **66**, 073202 (2002).
[10] E.-C. Lee and K. J. Chang, Phys. Rev. B **70**, 115210 (2004).
[11] M. G. Wardle, J. P. Goss, and P. R. Briddon, Phys. Rev. B **71**, 155205 (2005).
[12] A. M. Stoneham, J. Gavartin, A. L. Shluger, A. V. Kimmel, D. Muñoz Ramo, H. M. Rønnow, G. Aeppli, and C. Renner, J. Phys.: Condens. Matter **19**, 255208 (2007).
[13] A. L. Shluger and A. M. Stoneham, J. Phys.: Condens. Matter **5**, 3049 (1993).
[14] O. F. Schirmer, J. Phys.: Condens. Matter **18**, R667 (2006).
[15] J. L. Gavartin, P. V. Sushko, and A. L. Shluger, Phys. Rev. B **67**, 035108 (2003).
[16] R. Dovesi, R. Orlando, C. Roetti, C. Pisani, and V. R. Saunders, Phys. Status Solidi B **217**, 63 (2000).
[17] E. A. Kotomin, R. I. Eglitis, A. V. Postnikov, G. Borstel, and N. E. Christensen, Phys. Rev. B **60**, 1 (1999).
[18] D. Muñoz Ramo, A. L. Shluger, J. L. Gavartin, and G. Bersuker, Phys. Rev. Lett. **99**, 155504 (2007).
[19] D. Muñoz Ramo, J. L. Gavartin, A. L. Shluger, and G. Bersuker, Phys. Rev. B **75**, 205336 (2007).
[20] A. V. Kimmel, P. V. Sushko, and A. L. Shluger, J. Non-Cryst. Solids **353**, 599 (2007).
[21] C. H. Patterson, Phys. Rev. B **74**, 144432 (2006).
[22] X. Feng, J. Phys.: Condens. Matter **16**, 4251 (2004).
[23] P. Broqvist and A. Pasquarello, Appl. Phys. Lett. **89**, 262904 (2006).
[24] A. Alkauskas, P. Broqvist, and A. Pasquarello, Phys. Rev. Lett. **101**, 046405 (2008).
[25] A. Alkauskas, P. Broqvist, F. Devynck, and A. Pasquarello, Phys. Rev. Lett. **101**, 106802 (2008).
[26] F. Oba, A. Togo, I. Tanaka, J. Paier, and G. Kresse, Phys. Rev. B **77**, 245202 (2008).
[27] A. D. Becke, J. Chem. Phys. **98**, 1372 (1993).
[28] J. P. Perdew, M. Ernzerhof, and K. Burke, J. Chem. Phys. **105**, 9982 (1996).
[29] H. Heyd, G. E. Scuseria, and M. Ernzerhof, J. Chem. Phys. **118**, 8207 (2003).
[30] J. Muscat, A. Wander, and N. M. Harrison, Chem. Phys. Lett.

342, 397 (2001).
[31] J. Paier, M. Marsman, K. Hummer, G. Kresse, I. C. Gerber, and J. G. Angyan, J. Chem. Phys. **124**, 154709 (2006).
[32] R. Dovesi, V. R. Saunders, C. Roetti, R. Orlando, C. M. Zicovich-Wilson, F. Pascale, B. Civalleri, K. Doll, N. M. Harrison, I. J. Bush, Ph. D'Arco, and M. Llunell, CRYSTAL06 User's Manual, University of Torino, http://www.crystal.unito.it
[33] J. E. Jaffe and A. C. Hess, Phys. Rev. B **48**, 7903 (1993).
[34] M. D. Towler, N. L. Allan, N. M. Harrison, V. R. Saunders, W. C. Mackrodt, and E. Apra, Phys. Rev. B **50**, 5041 (1994).
[35] L. Ojamäe, K. Hermansson, C. Pisani, M. Causa, and C. Roetti, Acta Crystallogr., Sect. B: Struct. Sci. **50**, 268 (1994).
[36] R. Dovesi, C. Roetti, C. Freyria Fava, M. Prencipe, and V. R. Saunders, Chem. Phys. **156**, 11 (1991).
[37] S. C. Abrahams and J. L. Bernstein, Acta Crystallogr., Sect. B: Struct. Crystallogr. Cryst. Chem. **25**, 1233 (1969).
[38] R. D. Shannon, Acta Crystallogr., Sect. A: Cryst. Phys., Diffr., Theor. Gen. Crystallogr. **32**, 751 (1976).